nature materials

ARTICLES

PUBLISHED ONLINE: 14 SEPTEMBER 2015 | DOI: 10.1038/NMAT4407

Matrix elasticity of void-forming hydrogels controls transplanted-stem-cell-mediated bone formation

Nathaniel Huebsch[1,2,3†], Evi Lippens[1,2], Kangwon Lee[1,2†], Manav Mehta[1,2,4,5], Sandeep T. Koshy[1,2,3], Max C. Darnell[1,2], Rajiv M. Desai[1,2], Christopher M. Madl[1], Maria Xu[1], Xuanhe Zhao[1,6], Ovijit Chaudhuri[1,2,7], Catia Verbeke[1,2], Woo Seob Kim[1,2,8], Karen Alim[1], Akiko Mammoto[9], Donald E. Ingber[1,2,9], Georg N. Duda[4,5] and David J. Mooney[1,2*]

The effectiveness of stem cell therapies has been hampered by cell death and limited control over fate. These problems can be partially circumvented by using macroporous biomaterials that improve the survival of transplanted stem cells and provide molecular cues to direct cell phenotype. Stem cell behaviour can also be controlled *in vitro* by manipulating the elasticity of both porous and non-porous materials, yet translation to therapeutic processes *in vivo* remains elusive. Here, by developing injectable, void-forming hydrogels that decouple pore formation from elasticity, we show that mesenchymal stem cell (MSC) osteogenesis *in vitro*, and cell deployment *in vitro* and *in vivo*, can be controlled by modifying, respectively, the hydrogel's elastic modulus or its chemistry. When the hydrogels were used to transplant MSCs, the hydrogel's elasticity regulated bone regeneration, with optimal bone formation at 60 kPa. Our findings show that biophysical cues can be harnessed to direct therapeutic stem cell behaviours *in situ*.

Endogenous stem cell niches provide an optimal microenvironment for stem cell maintenance, and also facilitate stem cell deployment in response to host injury[1,2]. One particular niche component, the extracellular matrix (ECM), has been identified as a particularly important source of cues that direct cell fate decisions. Biomaterials have been designed to mimic these niches by presenting specific signalling cues to modulate stem cell expansion, migration and gene expression[2–5]. Incorporating these features may alleviate key drawbacks, including transplanted cell death, associated with cell-based therapies[6]. Biophysical aspects of the ECM, including elasticity, have been linked to a variety of cellular behaviours *in vitro* and *in vivo* using hydrogel systems[7–10]. However, current materials used to manipulate cell fate via matrix elasticity (for example, mechanotransduction) in three dimensions limit cell motility, proliferation or new tissue formation[8,11]. Materials used to elicit tissue formation via transplanted cells must also degrade to allow space for new tissue formation[12,13]. Unlike materials used to study mechanobiology *in vitro*, these transplantable, degradable scaffolds typically exhibit mechanical properties that change continuously over time, making it difficult to study relationships between matrix mechanics and cell behaviour. Slowly degrading macroporous sponges fabricated from polymers such as poly(lactide-co-glycolide) exhibit a structure compatible with tissue ingrowth[14], but these protein-fouling materials do not allow precise control of the cell–material interface, making it difficult to control transplanted cell behaviour through defined insoluble cues.

Void-forming hydrogels

To address the limitations of current materials, we developed void-forming hydrogels. Within these materials, cells are initially encapsulated into a nanoporous hydrogel milieu that subsequently form pores *in situ*, after injection into host tissues. Current techniques used to create macroporous biomaterials rely on extraction of porogen templates by solvents[7,15,16], *in situ* degradation of soft materials[17], phase inversion[18], cell-mediated degradation of single-phase hydrogels[19], or three-dimensional (3D) printing[20]. A significant drawback of scaffold-based methods is that they typically do not allow simple delivery of the material via injection. Although enzymatically degradable, single-phase hydrogel materials offer elegant control over cellular invasion, cell confinement within these systems remains strongly coupled to matrix elasticity, and enzyme-mediated changes to local mechanical properties may be difficult to control in a pre-determined manner. Exogenous mechanical stimulation of cells in 3D culture alters their matrix

[1]Harvard University School of Engineering and Applied Sciences, Cambridge, Massachusetts 02138, USA. [2]Wyss Institute for Biologically Inspired Engineering, Cambridge, Massachusetts 02138, USA. [3]Harvard-MIT Division of Health Sciences and Technology, Cambridge, Massachusetts 02139, USA. [4]Julius Wolff Institute, Charité—Universitätsmedizin Berlin, 13353 Berlin, Germany. [5]Berlin-Brandenburg Center for Regenerative Therapies, 13353 Berlin, Germany. [6]Massachusetts Institute of Technology, Department of Mechanical Engineering, Cambridge, Massachusetts 02139, USA. [7]Stanford University Department of Mechanical Engineering, Stanford, California 94305, USA. [8]Department of Plastic Surgery, College of Medicine, Chung-Ang University, Heuk Seok-Dong, Dong Jak-Gu, Seoul 156-755, Korea. [9]Vascular Biology Program, Departments of Pathology & Surgery, Boston Children's Hospital and Harvard Medical School, Boston, Massachusetts 02115, USA. †Present address: Gladstone Institute of Cardiovascular Disease, San Francisco, California 94158, USA (N.H.); Graduate School of Convergence Science and Technology, Seoul National University, Seoul 16229, Korea (K.L.). *e-mail: mooneyd@seas.harvard.edu

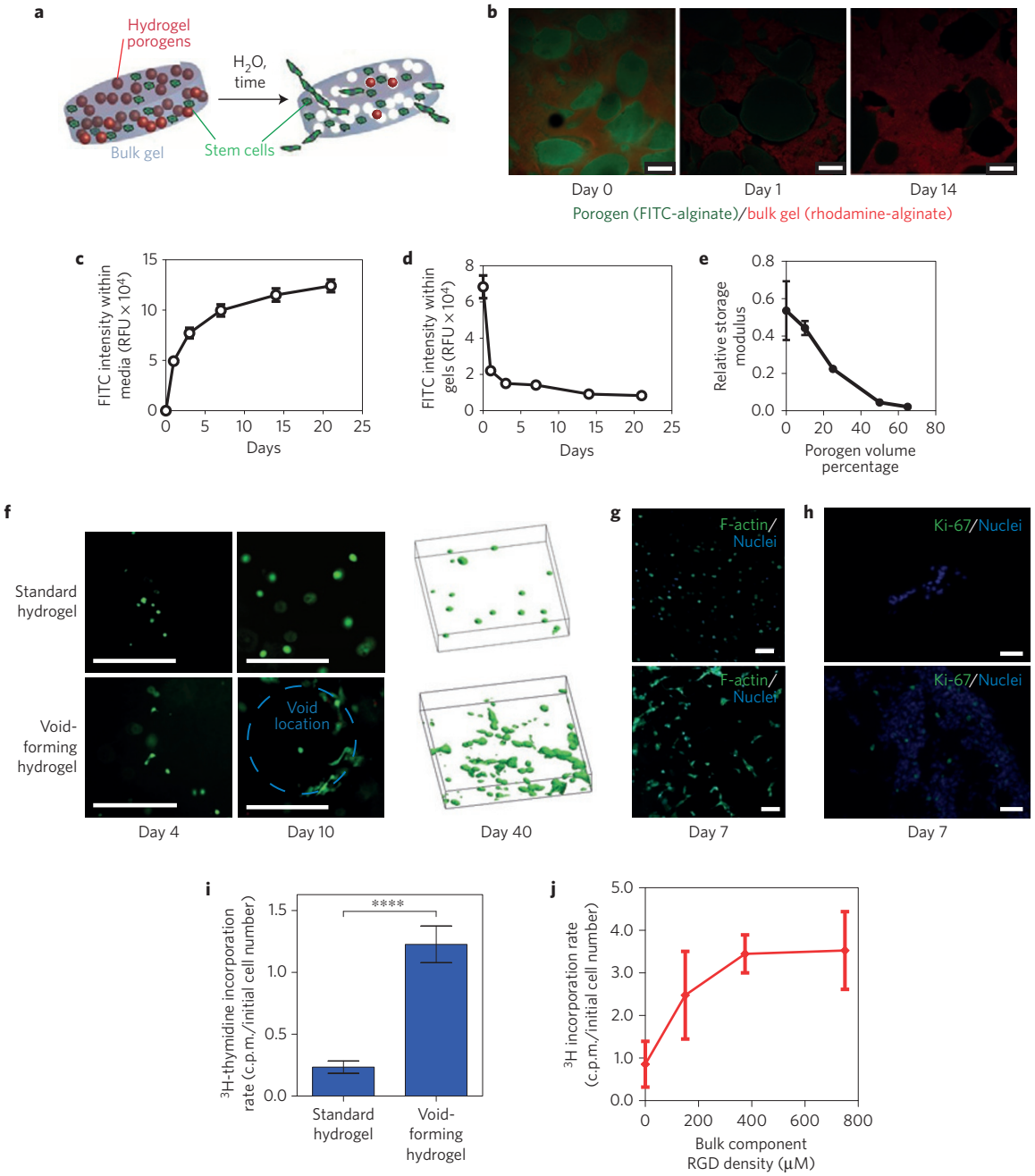

Figure 1 | Fabrication and characterization of void-forming hydrogels. a, Schematic of the strategy to create void-forming hydrogels. Porogens (red) and mesenchymal stem cells (green) are co-encapsulated into a bulk hydrogel (grey). Pores (white) form within the intact bulk hydrogel due to porogen degradation, allowing cell deployment out of the material and into damaged tissues. Note that the rate of cell migration out of the material is expected to be a function of the distance of the cells from the newly formed pores. **b**–**e**, Characterization of void-forming hydrogels. **b**, Confocal micrographs of aminofluorescein (FITC)-labelled porogens (green) within a rhodamine-labelled bulk gel (red), over the time course of porogen degradation. **c**,**d**, Quantitative analysis of the total level of fluorescein, proportional to porogen density, either remaining within gels (**c**) or dissolved in media bathing gels (**d**). Gels were dissolved in EDTA at set time points to quantify remaining label. **e**, Relative shear modulus G' of void-forming hydrogels as a function of volume fraction of porogen, one week after hydrogel fabrication. Values of G' are normalized to the value obtained for a standard hydrogel (no porogen) at day 1. Effects of porogen volume fraction on composite shear modulus were significant ($p < 0.05$, one-way analysis of variance (ANOVA)). **f**, Morphology of Calcein-AM-stained mMSC in standard hydrogels (top) or in void-forming hydrogels (bottom) at days 4 and 10 after encapsulation (dotted blue line denotes void location). Right: 3D projections of Calcein-AM-stained cells within either standard gels (top) or void-forming gels (bottom) after 40 days of *in vitro* culture. **g**, Representative confocal micrograph of mMSC stained with phalloidin (green, with Hoechst 33342 nuclear counterstain, blue) *in situ* within standard (top) and void-forming gels (bottom) at day 7. **h**, Representative micrographs depicting Ki67 expression (green, with Hoechst 33342 nuclear counterstain, blue) in 10 μm cryosections of mMSC in either standard gels (top) or void-forming gels (bottom) at day 7. **i**, 24 h ^{3}H-thymidine incorporation, in radioactivity counts per minute (c.p.m.), normalized to the initial cell number, by mMSC either in standard gels or void-forming hydrogels one week after encapsulation. **j**, 24 h ^{3}H-thymidine incorporation, in c.p.m., normalized to the initial cell number, by mMSC in void-forming hydrogels wherein the bulk component had a varied level of integrin-binding RGD peptides. RGD density had a significant effect on ^{3}H incorporation (one-way ANOVA). Error bars are s.d., $n = 4$ scaffolds. ****$p < 0.001$, two-tailed t-test. Scale bars: **b**, 1 mm; **f**,**h**, 100 μm; **g**, 20 μm.

metalloproteinase (MMP) activity[21], suggesting it is likely that mechanotransduction pathways triggered by the interaction of cellular contractile forces and matrix elasticity will also alter MMP activity in these hydrogel systems. In turn, this may make it difficult to decouple matrix elasticity from micron-scale cellular protrusion into the material.

We hypothesized that the aforementioned drawbacks could be overcome with a system wherein solid-phase porogens could be first encapsulated into a bulk hydrogel, but then degrade via hydrolysis, resulting in the creation of voids within the hydrogels after placement in physiologic conditions (Fig. 1a). Importantly, the rate of pore formation and subsequent cell release, endogenous cell infiltration and tissue formation would then be controlled by the rate of porogen degradation and cell migration and proliferation within pores. This would decouple the elasticity of the slowly degrading, 'bulk' component (Fig. 1a, grey) from cell confinement by the gel, with the rate of void formation and cell release pre-determined via the chemical composition of the porogens. Furthermore, these composite materials could be introduced into the body in a minimally invasive manner as long as the porogens within were smaller than the diameter of the injection needle.

To test the possibility of fabricating void-forming hydrogels, mechanically rigid, but rapidly degrading sacrificial gel porogens of an appropriate size (~150 μm diameter; Supplementary Fig. 1) were formed from oxidized, hydrolytically labile alginate[22], and encapsulated into a 'bulk' hydrogel comprised of slowly degrading, high molecular weight alginate (Fig. 1b and Supplementary Fig. 1). To assess the possibility of void formation *in situ*, we first performed scanning electron microscopy on composite gels that were flash-frozen in liquid nitrogen at different time points after formation. These studies suggested time-dependent void formation (Supplementary Fig. 2), but because of concerns about artefactual pore formation during freezing and lyophilization, we developed a fluorescence assay to directly analyse void formation within intact hydrogels (Fig. 1b). Simultaneous *in situ* fluorescence analysis of the porogens (green) and bulk component (red) of void-forming hydrogels revealed that porogens were initially intact, but degraded *in situ* to form voids (Fig. 1b). Quantifying the kinetics of porogen degradation revealed a timescale of approximately one week for the majority of porogen degradation (Fig. 1c,d). Consistent with these studies, rheological analysis of the shear modulus G' of these composite materials seven days after formation indicated a porogen-density-dependent decrease in G' in void-forming hydrogels, as compared to intact, standard hydrogels (not containing porogen) at day 0 (Fig. 1e). When the density of pores was above 50%, the relationship between pore concentration and the decrease of G' was nearly linear (Fig. 1e), consistent with theoretical predictions of the mechanical behaviour of pore-filled solids[23].

Cellular behaviour in void-forming hydrogels

The effects of pore formation on encapsulated cell morphology and distribution within the void-forming hydrogels were next analysed. Clonally derived mouse mesenchymal stem cells (mMSC; D1, ref. 24) were used as a cell model. Previous studies involving non-porous hydrogels indicate these cells and human MSC (hMSC) exhibit similar responses to matrix composition, but that D1 demonstrate less spontaneous osteogenic differentiation than primary human MSC (refs 6,25). The bulk phase of hydrogels was modified with peptides which present the integrin-binding RGD motif, to provide a defined mechanism for cell adhesion[26], and the density of porogens was held constant at 50% of the total volume of void-forming hydrogels. The overall morphology of mMSC was initially similar in standard and void-forming hydrogels. In contrast, after void formation, cells adjacent to pores exhibited extended distended, spread morphology (Fig. 1f), whereas cells in standard hydrogels, or those that were far from the pore phase within void-forming hydrogels, maintained a rounded morphology consistent with past reports[6,27]. Apparent changes in cell morphology were verified with phalloidin staining (Fig. 1g). Over longer time frames, pore formation led to enhanced cellularity and the presence of large cell clusters spanning significant distances within the composite material (Fig. 1f). This increase in apparent cellularity, although partly caused by morphology changes, was also due to cell proliferation. Proliferation could be controlled based on the dose of RGD presented by the bulk component of void-forming hydrogels (Fig. 1h–j). As cell encapsulation into alginate hydrogels is highly efficient and does not depend on RGD density (data not shown), these results indeed reflect the influence of RGD on cell proliferation (rather than initial cell density).

Given the ability to form void-forming hydrogels, and the interest in applying these materials to test the ability to use matrix elasticity to control transplanted-cell behaviour, we next performed *in vitro* studies to determine the effects on MSCs of modulating the elasticity of the RGD-modified bulk phase. At a fixed density of RGD peptides (375 μM), previously established to induce osteogenesis of hMSC in 3D culture[6], and a porogen volume density of 50%, mMSC proliferation and osteogenic commitment were analysed (Fig. 2). Cell proliferation exhibited a biphasic dependence on matrix elasticity, peaking within materials of intermediate stiffness (Fig. 2a). Osteogenic lineage commitment, assessed via alkaline phosphatase (ALP) activity in deployed cells, was also optimal with intermediate bulk matrix elasticity (Fig. 2b). These findings are consistent with previous work which indicated high levels of integrin occupancy occurred in 3D materials with intermediate elastic modulus[6]. Consistent with previous literature linking cell–matrix mechanics to differentiation of pre-osteoblasts[28], we observed a marked effect of matrix elasticity on mitogen-activated protein kinase (MAPK) signalling, as assessed by MAPK Thr202/Tyr204 phosphorylation within cells remaining in void-forming hydrogels after seven days of culture (Fig. 2c,d). To further verify the effect of bulk-component elasticity on the osteogenic behaviour of encapsulated MSC, more definitive markers of osteogenesis were assessed. Collagen I expression and mineralization by mMSC both occurred within void-forming hydrogels in an elasticity-dependent manner (Fig. 2e–g). These results are consistent with previous studies involving non-porous, RGD-modified cell-encapsulating hydrogels, which indicated a biphasic effect of elastic modulus, E, on osteogenesis[6], in materials that prevented cell migration and also limited proliferation. Normalizing collagen I expression to cell number did reveal a subtle effect of proliferation on total osteogenesis (Fig. 2h)—however, the biphasic relationship between matrix elasticity and osteogenic marker expression was preserved.

As the elasticity of the cell-interactive phase of void-forming hydrogels could be tuned to modulate MSC osteogenesis, we next investigated the application of these materials for cell deployment *in vitro*, to test their potential ability to support transplanted-cell deployment and ingrowth of newly formed endogenous tissue. As cell deployment was expected to occur via channels of interconnected voids spanning from the surface through the interior of the material, initial studies were performed to determine the minimum density of porogens required (Supplementary Methods). For infinitely large composite gels, a percolating network of porogens would be required, and this would lead to a minimum porogen volume fraction near 65%. However, given the ultimate size of gels used in these studies (2 mm diameter for *in vitro* studies, with injection volumes of 100 μl for *in vivo* studies), and the size of porogens (~150 μm diameter), numerical simulations predicted effective percolation of voids (a high likelihood of voids spanning through the material) with a porogen fraction of 50%. Although a volume fraction of 50% porogens was not sufficient for interconnected void formation as assessed by a capillary assay (Supplementary Methods and Supplementary Fig. 3), it was more

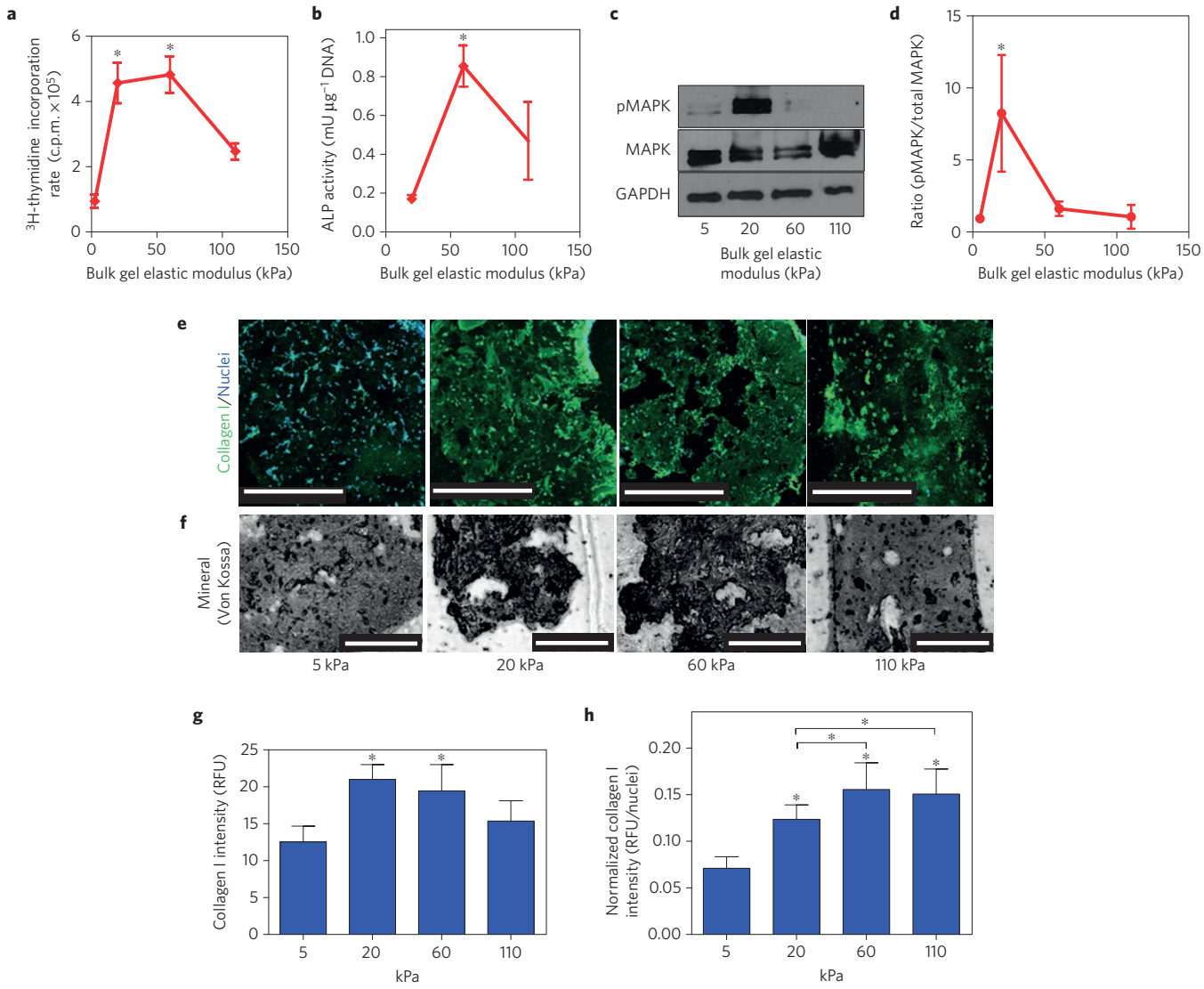

Figure 2 | Manipulating stem cell osteogenesis and proliferation by controlling the elasticity of the bulk phase of void-forming hydrogels. **a**, 24 h ^{3}H-thymidine incorporation, in radioactivity counts per minute (c.p.m.), by mMSC, after seven days of culture in void-forming hydrogels, as a function of the elastic modulus of the bulk component. RGD density of gels was constant (375 μM). **b**, Analysis of alkaline phosphatase (ALP; osteogenic biomarker) activity, normalized to the DNA density of mMSC deployed from void-forming hydrogels of varying bulk elastic modulus (375 μM RGD). Analysis was performed on cells that were released between days 7 and 14 of culture under osteogenic conditions. Bulk-gel elasticity had significant effects (one-way ANOVA) on both proliferation and ALP activity. **c**,**d**, Immunoblot analysis of MAPK phosphorylation (anti Phospho-p44/42 MAPK, Thr202/Tyr204) and total MAPK expression for mMSC within void-forming hydrogels as a function of bulk-component elasticity, seven days after gel formation, as depicted by a representative blot (**c**) and quantitative analysis (**d**). GAPDH was used as a loading control for western blots. **e**–**f**, Analysis of collagen I expression (green; Hoechst 33342 nuclear counterstain, blue) via antibody staining (**e**) and analysis of mineralization via Von Kossa staining (**f**), of mMSC within void-forming hydrogels of varying bulk-component elasticity, after 14 days of culture under osteogenic conditions. **g**–**h**, Quantification of average collagen I fluorescence signal from 16 cellular regions within the material either without (**g**) or with (**h**) normalization to the number of nuclei in each region. Matrix elasticity had a significant effect on collagen I levels (ANOVA). Error bars: s.d., $n = 3$–5 biologic replicates. $^*p < 0.05$, compared to 5 kPa condition, Holm–Bonferroni test, or $p < 0.05$ by 2-way t-test with Holm–Bonferroni correction for multiple comparisons. Scale bars: **e**,**f**, 400 μm.

than sufficient to allow cell release. Because this lower porogen volume fraction (50%) facilitated specimen handling, particularly with void-forming gels with a soft bulk component, this porogen density was used in all subsequent analyses.

The dependence of cell deployment kinetics on porogen material properties was next investigated. Cell deployment was monitored by measuring Alamar Blue reduction by cells that had deployed out of gels, onto the underlying plastic substrate, after verifying that this methodology produced similar estimates of cell release as direct, manual counts (Supplementary Fig. 3b). Pore formation led to substantial cell deployment from void-forming hydrogels, whereas little release occurred from standard gels with the same composition as the bulk component of void-forming hydrogels (Fig. 3a). The total number of cells deployed exceeded the number of cells initially encapsulated in the void-forming hydrogels, consistent with our previous observation of cell proliferation within these materials (Fig. 1h–j). Importantly, the kinetics of deployment and overall number of released cells could also be controlled by manipulating two porogen fabrication parameters: the concentration of hydrolytically labile groups in the polymers used to form porogens, and the concentration of divalent cation used to crosslink porogens (Fig. 3b,c). At a constant porogen

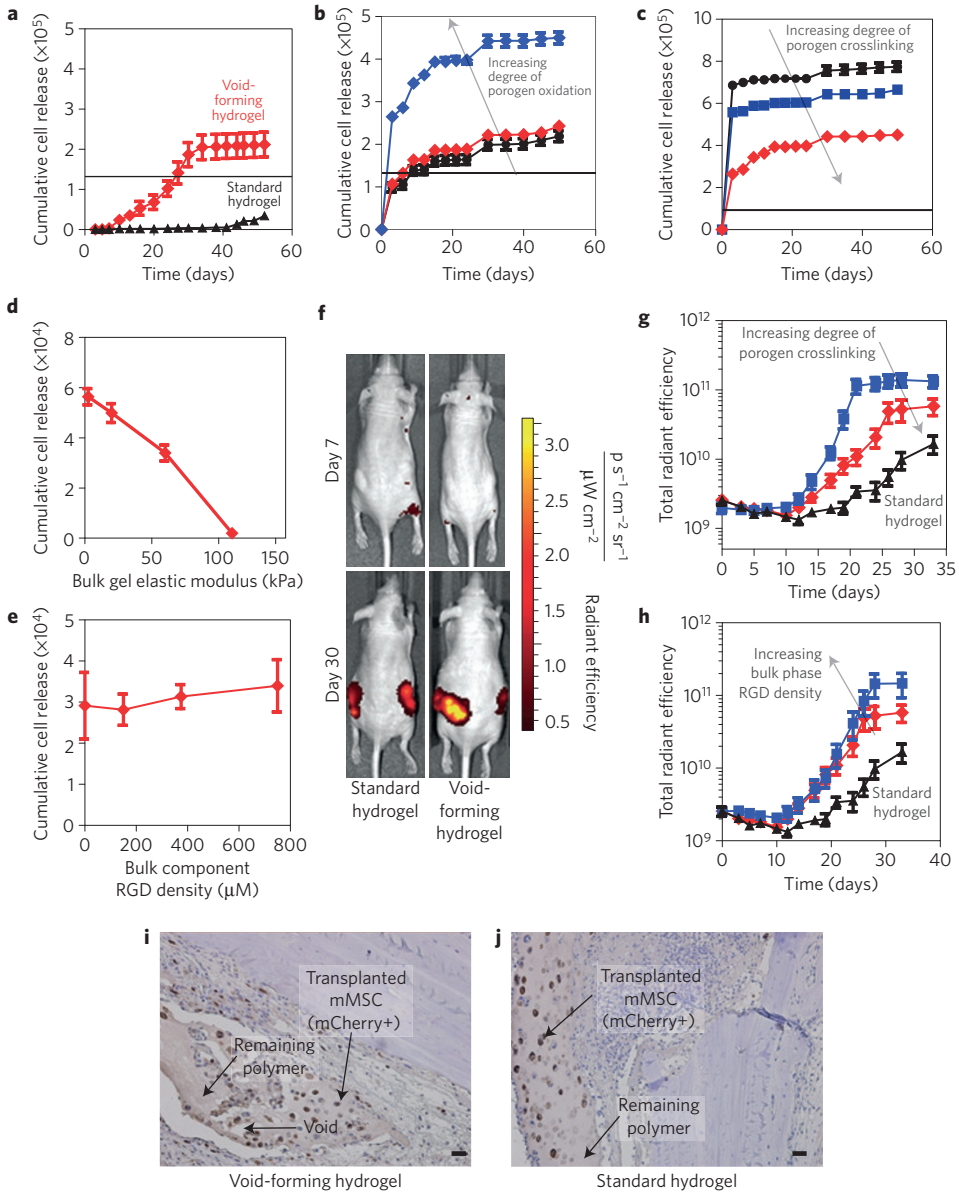

Figure 3 | Controlling cell deployment kinetics from void-forming hydrogels *in vitro* and *in vivo*. **a**, Kinetic analysis of mMSC deployment either from the bulk phase of void-forming hydrogels (red) or from standard nanoporous hydrogels (black). The horizontal black line denotes the number of cells initially encapsulated into each scaffold. Difference in net cell deployment between the two types of hydrogels was statistically significant ($p < 0.01$, two-tailed *t*-test) at all time points. **b**,**c**, Kinetics of mMSC deployment from the bulk phase of void-forming hydrogels as a function of porogen degradation rate, as manipulated by controlling the degree of oxidation of polymers used to form porogens (3% (black), 5% (red) or 7.5% (blue)) (**b**), or the concentration of calcium (25 mM (black), 50 mM (blue) or 100 mM (red)) used to crosslink porogens (**c**). Net cell deployment was significantly greater from materials with a 7.5% degree of porogen oxidation ($p < 0.001$ at all time points after day 0 by Holm–Bonferroni test) compared to deployment from materials with either 3 or 5% degree of oxidation. Each degree of porogen crosslinking yielded a level of net deployment that was statistically unique among the different materials tested at all time points after day 0 (Holm–Bonferroni test). **d**, Analysis of net mMSC deployment at day 7, as a function of the elasticity of bulk component of void-forming gels. Elasticity had a significant effect (one-way ANOVA) on cell deployment. **e**, Cumulative cell deployment for mMSC after one week of culture in void-forming gels with varying RGD peptide frequency. **f**, Representative images of Nu/J mice either 7 (top) or 30 (bottom) days after injection of standard (left) or pore-forming hydrogels (right) containing mCherry-expressing mMSC into the subcutaneous tissue. **g**, Total radiant efficiency (proportional to cell number) from mCherry-mMSC injected within the following hydrogels: void-forming gels with porogens crosslinked with either 100 mM (red) or 50 mM (blue) Ca^{2+}, or within standard hydrogels (black). Release of cells from either void-forming hydrogel yielded significantly more release than from a standard hydrogel at all time points beginning at day 10, and altering porogen fabrication had a significant effect on radiant efficiency beginning on day 17 ($p < 0.05$, two-tailed *t*-test). RGD density was fixed at 187 μM in the bulk-gel phase. **h**, Total radiant efficiency resulting from mCherry-mMSC injected within void-forming hydrogels in which the RGD concentration was either 187 μM (red) or 750 μM (blue) within the bulk phase, or within standard hydrogels (black). Cell transplantation within either void-forming hydrogel type led to substantially higher total radiant efficiency at all time points after day 12 (187 μM RGD) or 19 (750 μM RGD), compared to transplantation within standard hydrogels. The difference in total radiant efficiency was affected by the density of RGD presented by the bulk phase beginning on day 24 ($p < 0.05$). **i**,**j**, Representative micrographs of tissues in nude rat cranial defects one week after transplanting mCherry-mMSC with either void-forming (**i**) or standard hydrogels (**j**). mCherry antigen was probed with DAB chromogen. Error bars are s.e.m., $n = 3$–4 scaffolds (*in vitro* studies) or $n = 4$–8 scaffolds (*in vivo* studies). Scale bars: **i**,**j**, 100 μm.

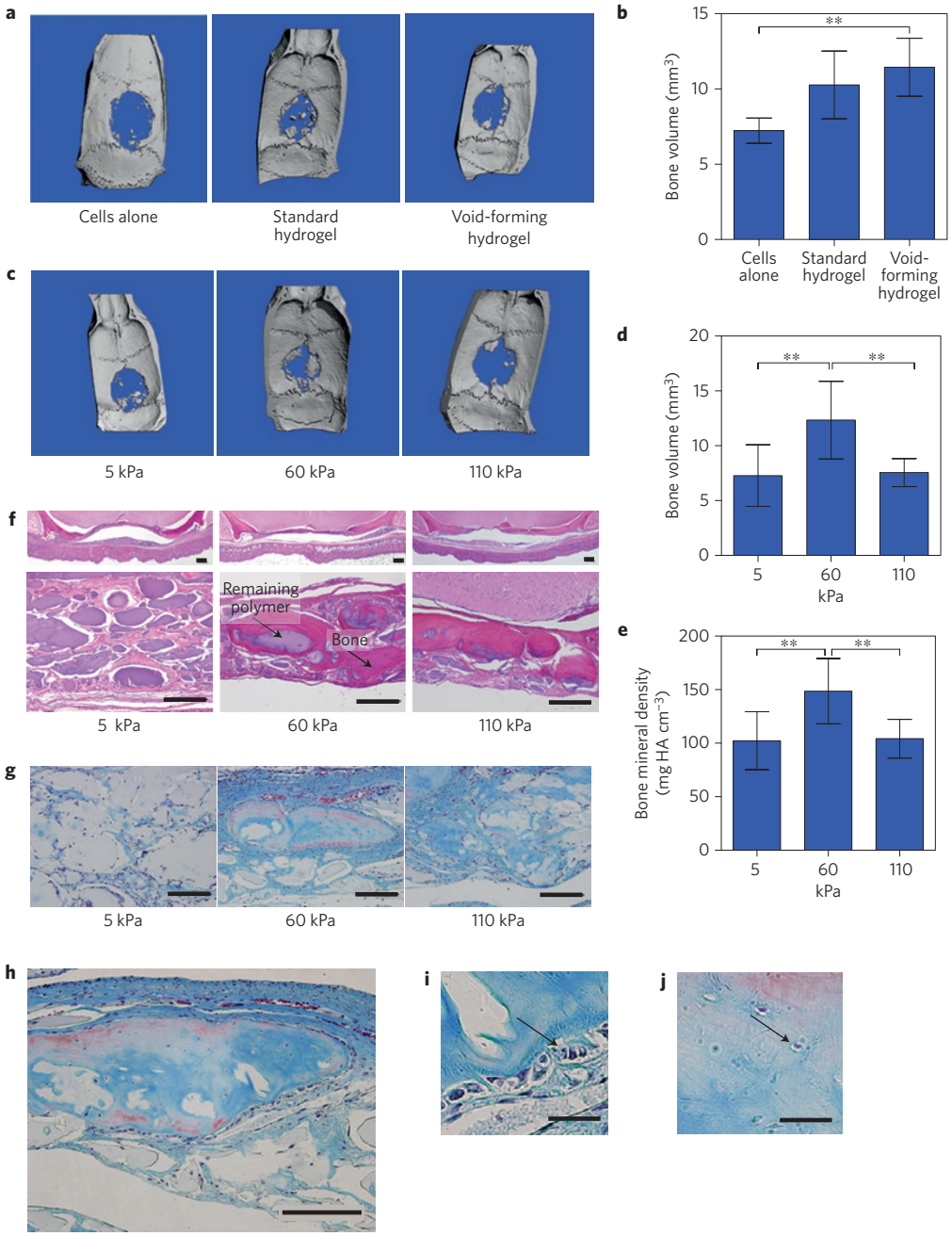

Figure 4 | Matrix elasticity regulates MSC-mediated bone regeneration. a,**b**, Analysis of bone regeneration in cranial defects due to hMSC transplantation via saline bolus, standard hydrogels or void-forming hydrogels. **a**, Representative micro-computed tomographic (μCT) images of regeneration in cranial defects in nude rats 12 weeks after introducing hMSC in saline (cells alone), within standard hydrogels or within void-forming hydrogels. **b**, Quantitative analysis of the total volume of newly formed bone tissue using μCT. **c**–**j**, Analysis of bone regeneration in cranial defects due to hMSC transplanted in void-forming hydrogels with different bulk-component elastic moduli. **c**, Representative μCT images of regeneration in nude rat cranial defects 12 weeks after hMSC delivery in void-forming hydrogels of varying bulk-component moduli. **d**,**e**, Quantitative analysis of total volume (**d**) and average bone mineral density (**e**) of regenerated bone. **f**, Representative histologic analysis of new bone formation and remaining polymer with haematoxylin–eosin staining. **g**, Representative Masson's trichrome staining depicting new bone formation. **h**–**j**, High-resolution micrographs depicting trichrome staining of a portion of newly regenerated tissue derived from hMSC transplanted in void-forming gels with a bulk modulus of 60 kPa. **h**, Entire sub-section. **i**,**j**, High-resolution images depicting osteoblast-like cells at the edge of newly forming tissue (**i**) and osteocyte-like cells in the central part of newly formed tissues (**j**) (denoted by black arrows). Error bars: s.d., $n = 4$–5. $^{**}p < 0.05$, two-tailed t-test. Scale bars: **f**–**h**, 100 μm; **i**,**j**, 20 μm.

density and RGD density (375 μM, the same density as used for *in vitro* osteogenesis assays), increasing the bulk-gel elasticity diminished cell deployment (Fig. 3d). Diminished cell release from materials with higher elastic moduli may reflect a higher adhesivity that prevents cell detachment[29], or an inability of the cells to deform the gels sufficiently to enable their migration through the material to access the pores[7]. Interestingly, net cell deployment from void-forming hydrogels with constant bulk-component elasticity (60 kPa) was not affected by RGD density (Fig. 3e). This is in contrast to previous work linking cell–ECM adhesiveness to cell migration speed[29]. The apparent discrepancy between these results may result from changes in cell migration speed being matched

by changes in cell proliferation, which substantially increased as the density of RGD peptides was raised from 0 to 750 μM. On the basis of this finding, it is most likely that modulating bulk matrix elasticity affected cell release by altering cells' ability to mechanically deform the hydrogel surrounding voids, as they migrate through the composite material.

Cell deployment from void-forming hydrogels *in vivo* was analysed using genetically labelled cells within hydrogels transplanted subcutaneously in nude mice. In the first week following cell transplantation, there was a slight (30%) decrease in the fluorescent signal from the mCherry-labelled mMSC for all transplantation conditions. Following this slight decrease, mMSC delivered within standard, nanoporous hydrogels were released to a modest extent, but only after several weeks (Fig. 3f,g and Supplementary Fig. 4), achieving a final density about 9.5 times higher than at day 7. However, mMSC delivered within void-forming hydrogels were released much more rapidly and proliferated markedly, over the same timescale on which pores formed, finally achieving a 31-fold increase over the density at day 7. Consistent with *in vitro* studies, both the overall number of mMSC and the kinetics of their deployment from pore-forming gels could be controlled by modulating porogen characteristics (Fig. 3g). Further, the number of deployed cells increased substantially when the density of peptides in the bulk gel was increased (Fig. 3h). Finally, within a cranial defect model, the generation of voids spanning the material and concomitant mMSC release could be detected histologically within one week of cell encapsulation within void-forming hydrogels (Fig. 3i). Cells released from these void-forming hydrogels were found at distances up to 350 μm away from the gels. In contrast, mMSC were retained in standard hydrogels (Fig. 3j).

Bone repair with void-forming hydrogels

As void-forming hydrogels could control MSC deployment, differentiation and proliferation *in vitro*, as well as expansion and dissemination of cells *in vivo*, we next investigated whether these materials could be used to enhance the effects of transplanted MSC on bone regeneration. Human MSC (hMSC), either in saline, standard hydrogels, or void-forming hydrogels, were directly injected into freshly formed critically sized cranial defects in nude rats. Both standard and void-forming hydrogels had a constant bulk composition (150 μM RGD, 60 kPa), which was chosen to match the properties of hydrogels previously demonstrated to elicit ectopic bone formation *in vivo* by encapsulated osteoblasts and chondrocytes[30]. Bone growth was evaluated 12 weeks after cell transplantation. Paralleling results from clinical studies involving direct stem cell transplantation[1], bolus delivery of hMSC alone in the nude rat model had only modest effects on bone regeneration, as measured by micro-computed tomography (Fig. 4a,b).

Transplantation of hMSC within standard, nanoporous hydrogels improved bone regeneration compared to the bolus injection group (Fig. 4b and Supplementary Fig. 5). hMSC transplantation within void-forming hydrogels led to a further, statistically significant increase in the amount of new bone formation, compared to cells alone (Fig. 4a,b). Histologic analysis revealed that when hMSC were delivered via saline bolus, much of the newly formed bone was near the margin of the original defect, probably reflecting ingrowth of tissue adjacent to the defect, rather than new bone formation (Supplementary Fig. 5). Delivery with nanoporous gels led to large masses of hydrogel remaining in the defect site, and the osteogenic tissue that had formed in this condition was often contained within the remaining hydrogel and not continuous with host tissues (Supplementary Fig. 5).

Compared to standard hydrogels, void-forming gels left a much smaller amount of remaining gel material 12 weeks following transplantation (Supplementary Fig. 5), and analysis of trichrome-stained sections also revealed the presence of osteoblasts emanating from the small fragments of residual material in void-forming gels near the centre of defects, consistent with the assumption that cells that directly interact with the material contributed to new bone formation (Supplementary Fig. 5). To determine the origin of the newly generated bone, we performed fluorescence *in situ* hybridization (FISH) studies to detect the primate specific Alu repeat mRNA sequence, on samples obtained after four weeks. Although mineralization had already occurred at this time point, it was less extensive than at 12 weeks, making FISH analysis feasible. At four weeks, although there were clearly detectable human cells remaining within both standard and void-forming hydrogels, the vast majority of cells were non-primate (rodent) in origin (Supplementary Fig. 5). These results suggest that transplanted cells either served as a source of osteogenic cytokines, or recruited endogenous rodent cells, which subsequently interacted with the gel to form bone. This hypothesis may be testable through the implantation of acellular hydrogels, either with or without cytokine loading. However, precisely matching cell-mediated cytokine delivery in terms of specific proteins and kinetics may prove challenging[31].

Finally, studies were performed to test the hypothesis that matrix elasticity regulates bone formation by transplanted stem cells. Strikingly, new bone formation exhibited a marked dependence on bulk matrix elasticity, with optimal regeneration occurring within materials with an intermediate elastic modulus (60 kPa; Fig. 4c–f). The volume of new bone generated with void-forming gels that did not exhibit this optimal elastic modulus was not statistically different from that of bone generated by transplanting cells in saline (Fig. 4a).

The effect of matrix elasticity on bone regeneration was found at 12 weeks, although the modulus of the material would be expected to diminish slightly by this time. This finding is consistent with previous data suggesting that MSC commit during their first one to two weeks in a mechanically optimal micro-environment, even if the mechanical cues vary after that time[5,6]. Moreover, MSC-derived cells that were cultured under these osteo-permissive 3D conditions *in vitro* were previously shown to elaborate osteogenic cytokines such as osteocalcin[6], and this may have contributed to fate decisions within transplanted hMSC and stimulation of bone formation by endogenous cells. Micro-computed tomographic (μCT) analysis of the bone mineral density and trichrome staining of tissue sections also suggested that the quality of newly formed bone was greatest at the intermediate bulk-gel stiffness (Fig. 4e–g). Finally, trichrome staining of sections derived from defects into which hMSC were delivered from hydrogels of optimal elasticity revealed newly formed bone with entrapped cells and osteoblasts on the bone surfaces, suggesting that tissue formation within the defect site mimics hallmarks of endogenous bone formation (Fig. 4h–j).

Outlook

The elastic modulus found in these studies to best induce bone formation and stimulate defect repair is similar to the optimal range found to induce osteogenic gene and protein expression in encapsulated MSC in nanoporous gels *in vitro*[6]. This suggests that mechanotransduction pathways that regulate stem cell gene and protein expression *in vitro* might be directly transferred to complex *in vivo* processes such as bone formation. Because the pore size of hydrogels used in that previous work were not permissive to cell migration or marked expansion, this result further suggests that at least part of the contribution of matrix elasticity to new bone formation is directly related to mechanically induced osteogenesis, and not simply secondary to the cells' ability to egress from gels. Furthering this notion that migration was not the sole determinant of mechanically controlled bone formation in the present study was our *in vitro* observation that MSC deployment was most pronounced in void-forming gels with a bulk-component elasticity

near 5 kPa—a range that was not compatible with new bone growth. Nevertheless, the bone repair we observed probably required some cell migration and proliferation, and the ability of hydrogels with elasticity in the 60 kPa range to support these processes (based on *in vitro* assays, Figs 2a,b and 3d) was also likely important for transplanted-cell-mediated tissue repair.

Previous *in vitro* work has demonstrated that with hydrogels that exhibit a high degree of swelling, changes in nanometre-scale ligand distribution resulting from changes in substrate crosslinking may have a more pronounced effect on MSC behaviour than do corresponding changes in matrix elasticity[32]. However, the results of the current study and other work with similar hydrogels that exhibit more limited changes in swelling, ligand density and nanometre-scale adhesion ligand distribution as elastic modulus is altered demonstrate direct effects of E on stem cell behaviour[6,33,34]. Recently developed materials in which secondary crosslinks can be formed *in situ*, or in which crosslinks can be degraded *in situ*, in the presence of cells, offer an elegant experimental approach to study temporal requirements for matrix elasticity to control cellular mechanotransduction *in vitro*[11,35,36]; however, causing void formation on the size scales required for cellular deployment out of, and infiltration into, these types of gels *in vivo* would require novel methodologies for precisely delivering light into tissues.

We have demonstrated that mechanotransduction, previously shown to regulate mesenchymal stem cell fate *in vitro*[5,6], and implicated in craniofacial development[37], can be harnessed to locally control stem-cell-mediated tissue repair *in situ*. Given the strong evidence that mechanotransduction pathways regulate a variety of other stem cell populations *in vitro*[33,38], we anticipate that these biophysical cues might be useful in regenerating other tissues. The optimal stiffness found to induce new bone growth in the present studies is slightly higher than that reported for *in vitro* osteogenesis in nanoporous 3D gels. However, MSCs near a newly formed pore likely experience a slightly diminished modulus compared to the stiffness sensed in nanoporous hydrogels[39], and this may underlie the small discrepancy. The finding that bone regeneration was initiated in the absence of exogenous growth factors suggests that these mechanotransduction pathways act synergistically with low basal endogenous levels of osteogenic cytokines[37,40]. Importantly, this suggests that optimally designed materials could be used to obtain highly localized control over transplanted-cell fate, preventing deleterious off-target effects that have previously been observed when high levels of locally administered osteogenic cytokines can diffuse out of the intended application area[41].

Given the promise of harnessing mechanotransduction towards transplanted-cell-mediated tissue repair, it will be important in future studies to define early changes in signalling and transcription networks that underlie later, functional changes in cell fate. In the present work, we identified a strong correlation between MAPK signalling and *in vitro* osteogenesis. However, the exact optimum for MAPK signalling (20 kPa) at day 7 differs from the optimum we observed for ALP activity and per-cell collagen I expression (60 kPa) at day 14. This suggests the potential need to glean quantitative information on multiple signalling pathways, over multiple time points, to predict matrix-guided MSC fate[42]. Likewise, precise identification of the timing of activation of osteogenic transcription factors (for example, Runx2, Osterix) would allow one to thoroughly explore the large variable space (elasticity, adhesion ligand density, rate of void formation, and so on) and identify optimal design parameters that induce the most efficient cell-mediated tissue repair.

We anticipate that void-forming hydrogels will provide a useful platform for future basic studies on cell–matrix interactions and translational studies involving cell therapies. Both the bulk hydrogel and porogen phases of these materials could be utilized in future work to deliver soluble cues to enhance regeneration. These materials could also be used to deliver inhibitory molecules (for example, function-blocking antibodies) to probe the molecular mechanisms through which cell–material interactions, or cellular interactions with host tissues, modify the fate of transplanted and endogenous cells[43]. Although not explored in the present work, the effects of biomaterial pore size on tissue formation and cell migration has been studied extensively in the past[7], and altering porogen size may facilitate enhanced control over endogenous cell recruitment in future studies. Furthermore, if the degradation properties of the bulk material are modified to yield more permanent structures (for example, by incorporating covalent rather than ionic crosslinking), these injectable materials may be useful towards preserving the survival and phenotype of human cells transplanted in the context of humanized models of *in vivo* stem cell niches (for example, bone marrow; ref. 44). In contrast to materials that require surgical implantation or that mediate significant protein adsorption (for example, poly(lactide-co-glycolide)), hydrogel materials used to fabricate void-forming gels may be less likely to induce inflammation or other processes that might interfere with the biology being analysed. By uncoupling several biophysical cues shown to regulate cell fate *in vitro*—including porosity, matrix elasticity and matrix adhesivity[7], the strategy used to fabricate void-forming hydrogels allows these variables to be independently tuned to control cell fate. The ability to harness these cues *in situ* will likely be useful for cell-based therapies, as well as basic studies on the biology of cell–matrix interactions *in vivo*.

Methods

Methods and any associated references are available in the online version of the paper.

Received 28 October 2013; accepted 31 July 2015; published online 14 September 2015

References

1. Wollert, K. C. & Drexler, H. Cell therapy for the treatment of coronary heart disease: A critical appraisal. *Nature Rev. Cardiol.* **7,** 204–215 (2010).
2. Silva, E. A., Kim, E. S., Kong, H. J. & Mooney, D. J. Material-based deployment enhances efficacy of endothelial progenitor cells. *Proc. Natl Acad. Sci. USA* **105,** 14347–14352 (2008).
3. Huebsch, N. & Mooney, D. J. Inspiration and application in the evolution of biomaterials. *Nature* **462,** 426–432 (2009).
4. Lutolf, M. P., Gilbert, P. M. & Blau, H. M. Designing materials to direct stem-cell fate. *Nature* **462,** 433–441 (2009).
5. Engler, A. J., Sen, S., Sweeny, H. L. & Discher, D. E. Matrix elasticity directs stem cell lineage specification. *Cell* **126,** 677–689 (2006).
6. Huebsch, N. *et al.* Harnessing traction-mediated manipulation of the cell/matrix interface to control stem-cell fate. *Nature Mater.* **9,** 518–526 (2010).
7. Peyton, S. R. *et al.* Marrow-derived stem cell motility in 3D synthetic scaffold is governed by geometry along with adhesivity and stiffness. *Biotechnol. Bioeng.* **108,** 1181–1193 (2011).
8. Scadden, D. T. The stem-cell niche as an entity of action. *Nature* **441,** 1075–1079 (2009).
9. Yang, F. *et al.* The effect of incorporating RGD adhesive peptide in polyethylene glycol diacrylate hydrogel on osteogenesis of bone marrow stromal cells. *Biomaterials* **26,** 5991–5998 (2005).
10. Mammoto, A. *et al.* A mechanosensitive transcriptional mechanism that controls angiogenesis. *Nature* **457,** 1103–1108 (2009).
11. Khetan, S. & Burdick, J. A. Patterning network structure to spatially control cellular remodeling and stem cell fate within 3-dimensional hydrogels. *Biomaterials* **31,** 8228–8234 (2010).
12. Hutmacher, D. W. Scaffolds in tissue engineering bone and cartilage. *Biomaterials* **21,** 2529–2543 (2000).
13. Simmons, C. A., Alsberg, E., Hsiong, S., Kim, W. J. & Mooney, D. J. Dual growth factor delivery and controlled scaffold degradation enhance *in vivo* bone formation by transplanted bone marrow stromal cells. *Bone* **35,** 562–569 (2004).
14. Ouyang, H. W., Goh, J. C. H., Thambyah, A., Teoh, S. H. & Lee, E. H. Knitted poly-lactide-co-glycolide scaffold loaded with bone marrow stromal cells in repair and regeneration of rabbit Achilles tendon. *Tissue Eng.* **9,** 431–439 (2003).

15. Madden, L. R. *et al.* Proangiogenic scaffolds as functional templates for cardiac tissue engineering. *Proc. Natl Acad. Sci. USA* **107,** 15211–15216 (2010).
16. Stachowiak, A. N., Bershteyn, A., Tzatzalos, E. & Irvine, D. J. Bioactive hydrogels with an ordered cellular structure combine interconnected macroporosity and robust mechanical properties. *Adv. Mater.* **17,** 399–403 (2005).
17. Golden, A. P. & Tien, J. Fabrication of microfluidic hydrogels using molded gelatin as a sacrificial element. *Lab Chip* **7,** 720–725 (2007).
18. Wang, H. *et al.* Biocompatibility and osteogeneesis of biomimetic nano-hydroxyapatite/polyamide composite scaffolds for bone tissue engineering. *Biomaterials* **28,** 3338–3348 (2007).
19. Lutolf, M. P. *et al.* Repair of bone defects using synthetic mimetics of collageneous extracellular matrices. *Nature Biotechnol.* **21,** 513–518 (2003).
20. Liu Tsang, V. *et al.* Fabrication of 3D hepatic tissues by additive photopatterning of cellular hydrogels. *FASEB J.* **21,** 790–801 (2007).
21. Prajapati, R. T., Chavally-Mis, B., Herbage, D., Eastwood, M. & Brown, R. A. Mechanical loading regulates protease production by fibroblasts in three-dimensional collagen substrates. *Wound Repair Regen.* **8,** 226–237 (2000).
22. Bouhadir, K. H. *et al.* Degradation of partially oxidized alginate and its potential application for tissue engineering. *Biotechnol. Prog.* **17,** 945–950 (2001).
23. Gibson, L. J. & Ashby, M. F. *Cellular Solids* (Cambridge Univ. Press, 1997).
24. Diduch, D. R., Coe, M. R., Joyner, C., Owen, M. E. & Balian, G. Two cell lines from bone marrow that differ in terms of collagen synthesis, osteogenic characteristics, and matrix mineralization. *J. Bone Joint Surg. Am.* **75,** 92–105 (1993).
25. Hsiong, S. X., Boontheekul, T., Huebsch, N. & Mooney, D. J. Cyclic RGD peptides enhance 3D stem cell osteogenic differentiation. *Tissue Eng. A* **15,** 263–272 (2009).
26. Rowley, J. A., Madlambayan, G. & Mooney, D. J. Alginate hydrogels as synthetic extracellular matrix materials. *Biomaterials* **20,** 45–53 (1999).
27. Benoit, D. S., Schwartz, M. P., Durney, A. P. & Anseth, K. S. Small functional groups for controlled differentiation of hydrogel-encapsulated human mesenchymal stem cells. *Nature Mater.* **7,** 816–823 (2008).
28. Khatiwala, C. B., Kim, P. D., Peyton, S. R. & Putnam, A. J. ECM compliance regulates osteogenesis by influencing MAPK signaling downstream of RhoA and ROCK. *J. Bone Miner. Res.* **24,** 886–898 (2009).
29. DiMilla, P. A., Stone, J. A., Quinn, J. A., Albelda, S. M. & Lauffenburger, D. A. Maximal migration of human smooth muscle cells on fibronectin and type IV collagen occurs at an intermediate attachment strength. *J. Cell Biol.* **122,** 729–737 (1993).
30. Alsberg, E., Anderson, K. W., Albeiruti, A., Rowley, J. A. & Mooney, D. J. Engineering growing tissues. *Proc. Natl Acad. Sci. USA* **99,** 12025–12030 (2002).
31. Frenette, P. S., Pinho, S., Lucas, D. & Scheirerman, C. S. Mesenchymal stem cell: Keystone of the hematopoietic stem cell niche and a stepping-stone for regenerative medicine. *Annu. Rev. Immunol.* **31,** 285–316 (2013).
32. Trappmann, B. *et al.* Extracelluar-matrix tethering regulates stem-cell fate. *Nature Mater.* **11,** 642–649 (2012).
33. Gilbert, P. M. *et al.* Substrate elasticity regulates skeletal muscle stem cell self-renewal in culture. *Science* **329,** 1078–1081 (2010).
34. Kong, H. J., Polte, T. R., Alsberg, E. & Mooney, D. J. FRET measurements of cell-traction forces and nano-scale clustering of adhesion ligands varied by substrate stiffness. *Proc Natl Acad. Sci. USA* **102,** 4300–4305 (2005).
35. Khetan, S. *et al.* Degradation-mediated cellular traction directs stem cell fate in covalently crosslinked three-dimensional hydrogels. *Nature Mater.* **12,** 458–465 (2013).
36. Yang, C., Tibbitt, M. W., Basta, L. & Anseth, K. S. Mechanical memory and dosing influence stem cell fate. *Nature Mater.* **13,** 645–652 (2014).
37. Mammoto, T. *et al.* Mechanochemical control of mesenchymal condensation and embryonic tooth organ formation. *Dev. Cell* **21,** 758–769 (2011).
38. Saha, K. *et al.* Substrate modulus directs neural stem cell behavior. *Biophys. J.* **95,** 4426–4438 (2008).
39. Sen, S., Engler, A. & J,Discher, D. E. Matrix strains induced by cells: Computing how far cells can feel. *Cell Mol. Bioeng.* **2,** 39–48 (2009).
40. Wang, Y. K. *et al.* Bone morphogenic protein-2 induced signaling and osteogenesis is Regulated by cell shape, RhoA/ROCK, and cytoskeletal tension. *Stem Cells Dev.* **21,** 1176–1186 (2012).
41. Axelrad, T. W. & Einhorn, T. A. Bone morphogenetic proteins in orthopaedic surgery. *Cytokine Growth Factor Rev.* **20,** 481–4882 (2009).
42. Platt, M. O., Wilder, C. L., Wells, A., Griffith, L. G. & Lauffenburger, D. A. Multipathway kinase signatures of multipotent stromal cells are predictive for osteogenic differentiation: Tissue-specific stem cells. *Stem Cells* **27,** 2804–2814 (2009).
43. Murry, C. E. & Keller, G. Differentiation of embryonic stem cells to clinically relevant populations: Lessons from embryonic development. *Cell* **132,** 661–680 (2008).
44. Groen, R. W. Y. *et al.* Reconstructing the human hematopoietic niche in immunodeficient mice: Opportunities for studying primary multiple myeloma. *Blood* **120,** e9–e16 (2012).

Acknowledgements

We thank S. Gunasekaran for assistance with sample cryosectioning, R. Choa for assistance with histologic analyses, and M. Brenner and V. Manoharan (Harvard University) for discussions on percolation. We thank K. Tomodo, P.-L. So and E. Hsiao (Gladstone Institute, San Francisco) for helpful discussions and editorial suggestions. We also acknowledge support from the Materials Research Science and Engineering Center (MRSEC, DMR-1420570) at Harvard University (D.J.M., X.Z., N.H.), funding from NIH (R37 DE013033), the Belgian American Educational Foundation (E.L.), an NSF Graduate Research Fellowship (N.H.), an Einstein Visiting Fellowship (D.J.M.) and funding of the Einstein Foundation Berlin through the Charité—Universitätsmedizin Berlin, Berlin-Brandenburg School for Regenerative Therapies GSC 203, the Harvard College Research Program (C.M.M., M.X.) and Harvard College PRISE, Herchel-Smith and Pechet Family Fund Fellowships (M.X.).

Author contributions

The experiments were designed by N.H., E.L. and D.J.M. and carried out by N.H., K.L., M.M., A.M., M.C.D., R.D., S.T.K., C.V., E.L., C.M.M., M.X., O.C., W.S.K. and X.Z. New reagents and analytical tools were provided by M.M., G.N.D., K.A., A.M. and D.E.I. The manuscript was written by N.H. and D.J.M. The principal investigator is D.J.M.

Additional information

Supplementary information is available in the online version of the paper. Reprints and permissions information is available online at www.nature.com/reprints. Correspondence and requests for materials should be addressed to D.J.M.

Competing financial interests

The authors declare no competing financial interests.

Methods

Void-forming hydrogels. To form the rapidly degrading porogen phase, high M_w, high guluronic acid (GA)-content alginates (MVG; FMC biopolymer) were modified by oxidation of between 3 and 7.5% of GA residues with sodium periodate (Sigma; ref. 21). Following dialysis, sterile filtration and lyophilization, binary mixtures of oxidized MVG combined with high M_w, unmodified MVG were dissolved into serum-free Dulbecco's Modified Eagle Media (DMEM; Invitrogen). Polymer solutions were formed into gel beads by extruding through a glass atomizer with co-axial nitrogen air flow at a constant pressure (30 mmHg) into a bath of 25–100 mM calcium chloride in 50–100 mM HEPES buffer (pH 7.4) with constant stirring. After 5 min of crosslinking, gel beads were retrieved, and washed to deplete excess calcium. In some cases, alginate polymers used to form porogens were labelled with aminofluorescein (Sigma; ref. 45) to facilitate analysis of porogen size and shape.

To form the slowly degrading, cell-interactive bulk-gel phase, MVG alginates were covalently coupled with the integrin-binding peptide $(Gly)_4$-Arg-Gly-Asp-Ala-Ser-Ser-Lys-Tyr (Peptides International; ref. 26). In studies involving the effects of bulk-gel elastic modulus on cells, RGD-modified MVG was combined with unmodified MVG or MVG that had been irradiated to reduce M_w but maintain crosslinking ability (ref. 46). Void-forming hydrogels were formed by encapsulating cells and porogens into the bulk-gel phase, and then crosslinking the bulk-gel phase with calcium sulphate. In some experiments, MVG used to form the bulk gel was labelled with tetramethylrhodamine cadaverine (Anaspec).

***In vitro* osteogenesis assays.** Clonally derived mouse mesenchymal stem cells (D1; ref. 24, used at passages 20-24. American Type Cell Culture, D1 ORL UVA [D1] (ATCC CRL-12424). Cells were verified to be free of mycoplasma by the manufacturer.) were encapsulated into the bulk-gel phase (20 million cells ml^{-1} of bulk gel, to mimic the density that would eventually be used for cranial defect studies) by mixing with polymer before addition of porogen beads and crosslinking. Immediately after crosslinking, composite hydrogels were transferred to tissue culture polystyrene substrates with DMEM containing 10% FBS and 1% penicillin/streptomycin. To facilitate osteogenesis, 50 μg ml^{-1} *L*-ascorbic acid and 10 mM β-glycerol phosphate were also added to the media, which was exchanged every two days. At 7 and 14 days, hydrogels were transferred aseptically to fresh media in a fresh tissue culture plate. Care was taken to avoid damaging hydrogels during transfer. After moving gels on day 14, wells in the used plate were washed with PBS and then adherent cells were lysed into a passive lysis buffer (Promega). The nuclear and cytosolic fractions were next separated by centrifugation (14,000*g*, 20 min). DNA was liberated from the nuclear pellet (CyQuant lysis buffer, Invitrogen), and quantified with Hoechst 33342, based on a standard curve generated with calf thymus DNA. Alkaline phosphatase (ALP) activity of the cytosolic fraction was quantified with 4-MUP reagent (Sigma), with a standard curve provided by calf intestine alkaline phosphatase (Sigma). In parallel with these studies, void-forming gels containing cells were fixed at day 14, first in paraformaldehyde (to fix cells) and then in barium chloride (to fix hydrogels). Samples were then embedded into optimal cutting temperature media (OCT) and flash-frozen in liquid N_2. 10 μm cryosections were then taken, which were stained with antibodies against collagen I (ab34710, Abcam), with Hoechst 33342 for nuclear counterstaining. Mineralization was assessed in 25 μm sections using Von Kossa staining. For immunoblot analysis of osteogenesis-related signalling in cells, on day 7 void-forming hydrogels were removed from culture and washed with PBS. Next, cells were retrieved from hydrogels via calcium chelation with ice-cold 500 mM EDTA. Cell pellets were washed in the same 500 mM EDTA solution, and the pellets were flash-frozen in liquid nitrogen. Cells were lysed directly into SDS sample buffer, and 50 μg of protein was resolved by SDS–PAGE, transferred to a nitrocellulose membrane and then probed with antibodies against phospho-MAPK Thr202/Tyr204 (Cell Signaling, #9101) or total MAPK (Cell Signaling, #4696). GAPDH (Millipore, #Mab374) was used as a loading control.

***In vitro* cell deployment and proliferation studies.** D1 mesenchymal stem cells (passages 20–24) were encapsulated into the bulk-gel phase (2 million cells ml^{-1} of bulk gel) by mixing with polymer before addition of porogen beads and crosslinking. Immediately after crosslinking, composite hydrogels were transferred to tissue culture polystyrene substrates with DMEM containing 10% FBS and 1% penicillin/streptomycin. Every 3–7 days, hydrogels were transferred aseptically to fresh media in a fresh tissue culture plate. Care was taken to avoid damaging hydrogels during transfer. Wells in the used plate were washed with PBS and then deployed cells that had adhered to the substrate were quantified via Alamar Blue assay (Invitrogen). A standard curve formed by plating serial dilutions of D1 cells was used to convert Alamar Blue reduction rates into cell numbers. The validity of this approach was tested at early time points through direct comparison of cell counts obtained by Alamar Blue to cell counts obtained by trypsinizing cells and counting with a haemocytometer (Supplementary Fig. 3).

***In vivo* cell deployment studies.** All animal studies were performed under protocols approved by institutional guidelines (Harvard University Institutional Animal Care and Use Committee). D1 cells were transduced using pOC-mCherry retrovirus[10]. Cells were then encapsulated into the bulk phase of void-forming hydrogels, and composite gels were injected (2×10^6 cells per 100 μl injection) into the subcutaneous space in the flank of Nu/J mice (Jackson) via 18-gauge needles. Each mouse received two bilateral injections. Over the time course of the study, the overall level of mCherry fluorescence, proportional to cell density, was measured using a Caliper Life Sciences IVIS Xenogen imaging system. Animals were anaesthetized with isoflurane during imaging procedures. All animal experiments were performed according to established animal protocols. For studies of cell deployment within cranial defects, 8-mm critical-sized cranial defects were formed in nude rats (Charles River), and a constant volume of hydrogel (100 μl) containing 2 million mCherry-expressing D1 was injected directly into the freshly formed defect. One week after transplantation, animals were euthanized, mineralized bone was decalcified (EDTA), and histologic sections were acquired which encompassed the defect area. Transplanted D1 were identified by immunohistochemical staining for mCherry (AbCam, 10 μG ml^{-1}) visualized by DAB chromogen (Thermoscientific) on a background of tissue stained with haematoxylin.

Cranial defect studies. Human MSC (hMSC) (Poietics human mesenchymal stem cells) were purchased from Lonza and verified to be free of mycoplasma by the manufacturer. hMSC were propagated in low glucose DMEM with 20% FBS and 1% penicillin/streptomycin to passage 2–6. Subsequently, cells were encapsulated into the bulk phase of void-forming hydrogels or standard hydrogels, or mixed into saline. Cranial defects were formed as described above, and a constant volume of hydrogel or saline (100 μl) containing 2 million hMSC was delivered into the freshly formed defects. After the surgeries, animals were encoded so that μCT and histology could be performed in a blinded fashion. Animals were euthanized after 12 weeks, and bone regeneration was detected using μCT on a Viva40 (Scanco Medical, AG), at a voltage of 55 kV and current of 145 μA, integration time of 314 ms. The voxel size was selected to be isotropic and fixed at 35.5 μm. The scan axis was adjusted to be normal to the subject frontal plane. An established protocol for quantitative analysis of μCT scans was used to obtain measurements of the bone volume and average mineral density of newly formed mineral within defects (ref. 47).

References

45. Kong, H. J., Chan, J. H., Huebsch, N., Weitz, D. & Mooney, D. J. Noninvasive probing of the spatial organization of polymer chains in hydrogels using fluorescence resonance energy transfer (FRET). *J. Am. Chem. Soc.* **129,** 4518–4519 (2007).
46. Kong, H. J., Smith, M. K. & Mooney, D. J. Designing alginate hydrogels to maintain viability of immobilized cells. *Biomaterials* **24,** 4023–4029 (2003).
47. Mehta, M., Checa, S., Lienau, J., Hutmacher, D. & Duda, G. N. *In vivo* tracking of segmental bone defect healing reveals that callus patterning is related to early mechanical stimuli. *Eur. J. Cell. Mater.* **24,** 358–371 (2012).